Physica B 630 (2022) 413674

Contents lists available at ScienceDirect

Physica B: Physics of Condensed Matter

journal homepage: www.elsevier.com/locate/physb

Effect of native point defects on the photocatalytic performance of $ZnIn_2S_4$

Siwakorn Sukharom [a], Adisak Boonchun [a,b], Pakpoom Reunchan [a,b], Sirichok Jungthawan [b,d,c], Sukit Limpijumnong [b,e], Jiraroj T-Thienprasert [a,b,*]

[a] Department of Physics, Faculty of Science, Kasetsart University, Bangkok, 10900, Thailand
[b] Thailand Center of Excellence in Physics, Ministry of Higher Education, Science, Research and Innovation, 328 Si Ayutthaya Road, Bangkok, 10400, Thailand
[c] School of Physics, Institute of Science, Suranaree University of Technology, Nakhon Ratchasima, 30000, Thailand
[d] Center of Excellence in Advanced Functional Materials, Suranaree University of Technology, Nakhon Ratchasima, 30000, Thailand
[e] The Institute for the Promotion of Teaching Science and Technology, Bangkok, 10110, Thailand

ARTICLE INFO

Keywords:
Photocatalyst
First-principles calculations
Defect

ABSTRACT

Understanding of materials at atomic scale is mandatory for improving their physical properties in the desired way. Here, first-principles calculations with the most accurate hybrid functional are performed to investigate one of the most attractive photocatalyst $ZnIn_2S_4$. The electronic structures of perfect and defective cubic-$ZnIn_2S_4$ are examined as a representative of other $ZnIn_2S_4$ polymorphs. The influence of growth conditions on the photocatalytic activity of $ZnIn_2S_4$ is elucidated by considering the formation energy of native point defects under different growth conditions. Our results reveal that undoped $ZnIn_2S_4$ is a native *n*-type material owning to the high pinned Fermi-level under all growth conditions. The source of electron carriers in undoped $ZnIn_2S_4$ is the In_{Zn} antisite defect and its photocatalytic performance is declined by the formation of dominant compensating Zn vacancy defect. The S-poor growth condition of undoped $ZnIn_2S_4$ is unveiled to provide the best photocatalytic performance due to the highest pinned Fermi-level.

1. Introduction

Synthetic dyes are extensively used in various modern industry, including plastic, leather, and textile [1]. However, the wastewater released from these industries has serious effect on the water contamination causing severe environment concern because many of synthetic dyes are toxic to human as well as animal. In addition to water contamination, the increase of greenhouse gas CO_2 caused by the utilization of fossil fuels has also raised environmental concern. Several technological systems have been developed to treat the wastewater from industry as well as to reduce CO_2 to fuels or value-added chemicals. Among them, photocatalyst is a promising green-approach for environmental remediation as well as energy conversion [2–5]. Owning to its high efficiency, low-cost, chemical stability and photo-corrosion resistance, the photocatalyst is widely used to decompose synthetic dyes as well as organic pollutants by utilizing a solar energy, which is free and inexhaustible [6–9]. This leads to a sustainable option for environmental remediation. The commonly used photocatalyst Titanium dioxide has a large bandgap of ~3.3 eV, which limits its utilization to ultraviolet light region being a small fraction of sun light. The crucial parameter for selecting photocatalyst materials is not only the band gap, but also the band edges positions. Consequently, numerous efforts have been devoted to the exploration and development of new visible-light responsive photocatalysts to improve the photocatalytic activity [10–13].

The photocatalyst $ZnIn_2S_4$ has attracted much attention due to its excellent photocatalytic activity for water splitting and decomposition of organic contaminants under visible light [14–17]. $ZnIn_2S_4$, which is a ternary chalcogenide, can crystalize in two different polymorphs based on cubic and hexagonal lattices [18]. Numerous synthesis methods have been reported to synthesize $ZnIn_2S_4$ with difference morphologies as well as difference polymorphs [17,19–21]. Both hexagonal and cubic $ZnIn_2S_4$ phases were successfully synthesized, and their photocatalytic performances were investigated. It has been revealed that different polymorphs gave different effect on the photocatalytic performance for the degradation of organic dyes and the reduction of CO_2 [17,21]. However, the photocatalytic activity of undoped $ZnIn_2S_4$ is still low due to the poor light absorption and the recombination of photoinduced charge carriers. Several attempts have been carried out to enhance the photocatalytic performance of $ZnIn_2S_4$. To enhance the light absorption,

* Corresponding author. Department of Physics, Faculty of Science, Kasetsart University, Bangkok, 10900, Thailand.
E-mail address: chorawut.t@ku.th (J. T-Thienprasert).

https://doi.org/10.1016/j.physb.2022.413674
Received 22 October 2021; Received in revised form 27 December 2021; Accepted 5 January 2022
Available online 10 January 2022

some metal-doped $ZnIn_2S_4$ were synthesized to improve the visible-light absorption [22–25]. To inhibit the recombination of photoinduced charge carriers, $ZnIn_2S_4$ based composite photocatalysts have been developed such as $CuO/ZnIn_2S_4$ [19], $CdS/ZnIn_2S_4$ [26], $In_2S_3/ZnIn_2S_4$ [27], and cubic quantum dot/hexagonal $ZnIn_2S_4$ [28]. Recently, Xingchen J. et al. reported that the hexagonal-$ZnIn_2S_4$ grown under Zn poor condition can greatly enhance the photocatalytic activity due to the generated trap states related to Zn vacancies [29]. Further, Shuqu Z. et al. revealed that S vacancies in $ZnIn_2S_4$ acts as an electron traps prevented vertical transmission of electrons and enhanced electrons onto the Zn facet [30]. To the best of our knowledge, the theoretical study of native point defects in both cubic and hexagonal $ZnIn_2S_4$ phases has never been reported. Due to the higher symmetry of cubic-$ZnIn_2S_4$ over hexagonal-$ZnIn_2S_4$, we first selected to investigate the native point defects in cubic phase, which requires less computational demands, and we believed that the behaviors of the native point defects in cubic polymorph should resemble those in hexagonal polymorph as previously reported in anatase-TiO_2 and rutile-TiO_2 [31,32]. It is clearly seen that the crystal structures of anatase-TiO_2 (wurtzite) and rutile-TiO_2 (cubic) are difference; however, the dominant native point defects in both structures are still analogous.

In this paper, first-principles calculations with the most accurate hybrid functional were carried out to investigate the electronic properties of perfect and defective cubic-$ZnIn_2S_4$. The formation energies of all native point defects under several growth conditions were calculated to understand the effect of native point defects on its photocatalytic activity under different growth conditions. The calculated results were discussed along with the relevant experiments.

2. Computational details

We employed first-principles density functional theory calculations with hybrid functional and a plane wave basis set as implemented in Vienna ab-initio simulation package (VASP version 5.4.4) [33–35]. The projector augmented wave method (PAW) was carried out to explain the interaction between ions and electrons [36]. The most accurate hybrid functional proposed by Heyd, Scuseria, and Ernzerhof (HSE06) was performed for describing the exchange-correlation energy [37,38]. The cutoff energy for expanding the plane-wave basis set was set at 400 eV. For bulk cubic-$ZnIn_2S_4$ calculations, Monkhorst-Pack scheme with a sampling mesh points of $6 \times 6 \times 6$ were used for *k*-space integration [39]. All atoms in the cell were fully allow to relax until the Hellmann-Feynman forces [40] became less than 0.01 eV/Å. The amount of nonlocal Fock-exchange of 25% was set according to HSE06 scheme, which provides the calculated band gap of 2.39 eV. This is in good agreement with the experimental band gap of 2.34 eV [21]. Further, the calculated lattice parameter of 10.681 Å is in good agreement with the experimental values of 10.590 Å [41]. It is clearly seen that the calculations with HSE06 functional provide excellent details of crystal and electronic structures of cubic-$ZnIn_2S_4$; indicating the high reliability of our calculated approach.

To investigate the native point defects in cubic-$ZnIn_2S_4$, we used a supercell approach [42,43] with a supercell size of 112 atoms, which is constructed by repeating the 14-atom cubic-$ZnIn_2S_4$ unit cell in *a*, *b*, and *c* directions by $2 \times 2 \times 2$ as illustrated in Fig. 1. The spurious interactions causing by the defects in the periodic neighboring cells should be suppressed due to this large supercell size. For defect calculations, the sampling *k*-point mesh was reduced to $1 \times 1 \times 1$ shifted from Γ point and all atoms in the supercell were allowed to move until the residual forces acting on each atom became less than 0.02 eV/Å; resulting in the lowest

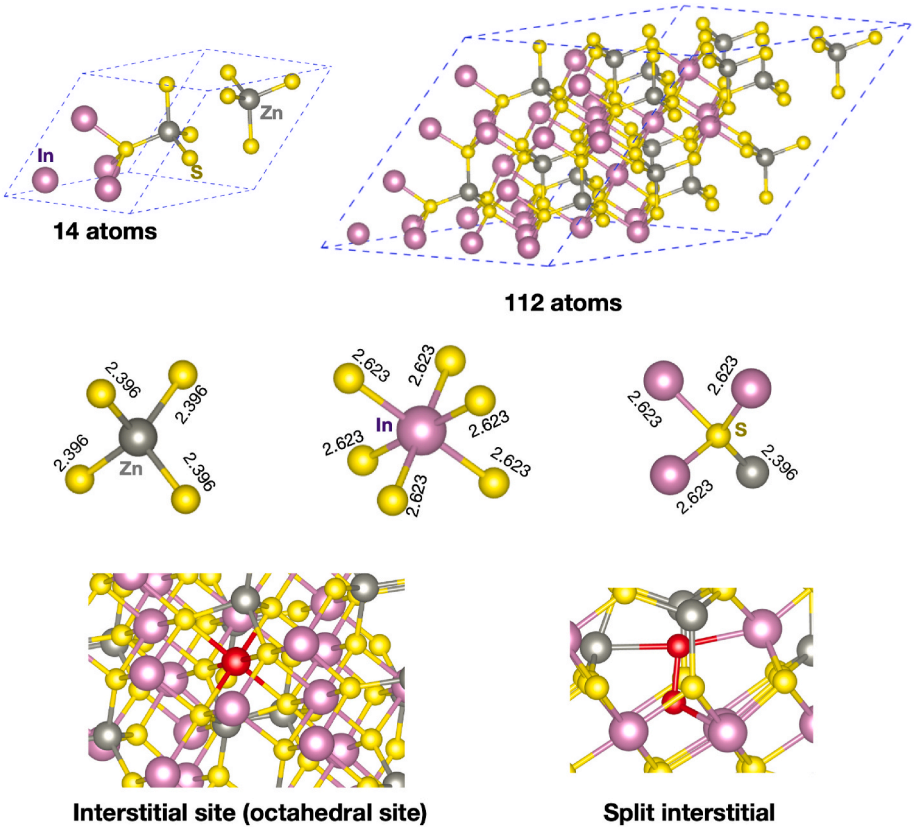

Fig. 1. Cubic-$ZnIn_2S_4$ structure with 14-atom primitive cell, 112-atom supercell and their local structures. The bond length is showed in angstrom unit. The grey, purple, and yellow ball represent Zn, In, and S, respectively. The octahedral and split interstitial sites are depicted in the lowest part by a red ball. (For interpretation of the references to colour in this figure legend, the reader is referred to the Web version of this article.)

energy configuration for each defect. The spin-polarized calculations were included for all defect calculations.

2.1. Defect formation energy

In principle, the concentration of defect at any temperature can be written in the form of Boltzmann distribution by

$$C(D^q) = \exp\left(-\frac{E_f(D^q)}{k_B T}\right), \quad (1)$$

where k_B and T is the Boltzmann constant and temperature, respectively, and $E_f(D^q)$ is the formation energy of defect D at charge state q. This equation implies that the lower formation energy of defect, the higher concentration of defect we obtain. The formation energy of defect is defined by

$$E_f(D^q) = E_{tot}(D^q) - E_{tot}(bulk) + \sum_i n_i\mu_i + q(E_F + E_{VBM}) + \Delta_q \quad (2)$$

where $E_{tot}(D^q)$ and $E_{tot}(bulk)$ are the total ground state energy of supercell with the defect D in charge state q and without any defect, respectively. n_i is the number of atom being added or removed to create the defect D in the supercell, μ_i is the atomic chemical potential associated with the added or removed atoms as described below, E_F is the Fermi energy referenced to the valence band maximum (E_{VBM}), and the last term Δ_q is the finite-size correction term, which is proposed by Freysoldt, Neugebauer, and Van de Walle, which is known as FNV method [37,38].

For some defect, it would exist in more than one stable charge state creating the energy level inside the band gap. We can then determine this energy level, called defect transition level $\varepsilon(q_1/q_2)$, associated with each defect from the following equation

$$\varepsilon(q_1/q_2) = \frac{E_f(D^{q_2}) - E_f(D^{q_1})}{q_1 - q_2} \quad (3)$$

where $E_f(D^{q_1})$ and $E_f(D^{q_2})$ are the formation energy of defect D in charge state q_1 and q_2, respectively. The shallow or deep state can be interpreted from this level.

2.2. Chemical potential

From equation (2), it is obviously seen that the formation energy of defects directly depends on their chemical potentials as well as Fermi-level of the system. In principle, Fermi-level can be any values varying between VBM and conduction band minimum (CBM). Regarding the chemical potentials, we must consider the phase stability diagram to determine all possible values of chemical potentials. To grow a single crystal cubic-$ZnIn_2S_4$, the following condition must be satisfied

$$\mu_{ZnIn_2S_4} = \mu_{Zn} + 2\mu_{In} + 4\mu_S, \quad (4)$$

where $\mu_{ZnIn_2S_4}$ is the heat of formation per formula unit of cubic-$ZnIn_2S_4$, μ_{Zn} μ_{In}, and μ_S are the chemical potentials for Zn, In and S atoms, respectively. In addition, more constraints need to be applied to Eq. (4) to prevent the formation of undesired phases, including metallic Zn (HCP), metallic In (FCC), metallic S (orthorhombic), InS, In_2S_3, ZnS, and ZnS_2 as summarized below;

$$\mu_{Zn} < E_{tot}(metallic - Zn),\ \mu_{In} < E_{tot}(metallic - In),\ \mu_S < E_{tot}(metallic - S),$$
$$\mu_{In} + \mu_S < E_{tot}(InS),\ 2\mu_{In} + 3\mu_S < E_{tot}(In_2S_3),$$
$$\mu_{Zn} + \mu_S < E_{tot}(ZnS),\ \mu_{Zn} + 2\mu_S < E_{tot}(ZnS_2), \quad (5)$$

where $E_{tot}(X)$ represents the heat of formation per formula unit of X phase (X can be metallic-Zn/In/S or InS or In_2S_3 or ZnS or ZnS_2). To illustrate all possible values of chemical potentials satisfied by Eq. (4) and Eq. (5), we simplify the three-dimension plot to two-dimension (2D) plot by projecting the chemical potential of S onto Zn-In plane as demonstrated in Fig. 2. The chemical potentials for Zn, In, and S can be any values lying on the shaded area. We note that all values shown in Fig. 2 are referenced to their natural phases, *i.e.*, metallic-Zn, metallic-In, and metallic-S. As mentioned before, the defect formation energy directly depends on their chemical potentials. To illustrate the dependence of defect formation energy under different growth conditions, we roughly selected three points marked by *a*, *b*, and *c* in Fig. 2 as a representative for S-poor, S-mid, and S-rich growth conditions. Note that S-mid represents an averaged condition between S-poor and S-rich growth conditions.

3. Results and discussion

3.1. Crystal and electronic properties of bulk cubic-$ZnIn_2S_4$

The relaxed crystal structure of 14-atom cubic-$ZnIn_2S_4$ primitive cell are depicted in Fig. 1. We note that the primitive cell shown in Fig. 1 is exactly equivalent to the cubic structure with space group $Fd\bar{3}m$. Their local environments around Zn, In, and S are also illustrated at the lower part of Fig. 1. It is found that Zn is four-fold coordinated to S atoms, while In is six-fold coordinated to S atoms. All the four Zn-S and six In-S bond lengths in cubic-$ZnIn_2S_4$ are equal with the bond lengths of 2.396 and 2.623 Å, respectively. Regarding S atom, it is four-fold coordinated to three In atoms and one Zn atom as depicted in Fig. 1. It can be seen that Zn-S bonds are shorter than In-S bonds indicating stronger interactions between Zn and S atoms. It is clearly seen that the cubic-$ZnIn_2S_4$ has higher symmetry structure than hexagonal-$ZnIn_2S_4$. Therefore, the calculations of defects in cubic structure would take less computational time than those in hexagonal structure. Further, it has been reported that the investigation of defects in anatase-TiO_2, which is hexagonal-based structure, provides analogous results as those obtained in rutile-TiO_2 [31,32]. Consideration of cubic-based structure would help reducing the computational demands, especially for HSE06 functional calculations.

The electronic band structures and projected density of states of cubic-$ZnIn_2S_4$ are illustrated in Fig. 3, in which VBM is set to zero. It is revealed that cubic-$ZnIn_2S_4$ is an indirect band gap with the calculated energy gap of ~2.39 eV in good agreement with the experimental bandgap of 2.34 eV [21] and the CBM and VBM are located at Γ and K points, respectively. Recently, it has been reported that the calculated energy gaps of cubic-$ZnIn_2S_4$ with GGA and GGA + U functionals are 1.08 and 1.18 eV, respectively, while those with mBJ-GGA and mBJ-GGA + U functionals provided the larger band gaps of 2.52 and 2.59 eV, respectively [44]. It is obviously seen that the calculated band gaps of cubic-$ZnIn_2S_4$ strongly depend on the functional used in the calculations. However, it is obviously seen that HSE06 functional, which

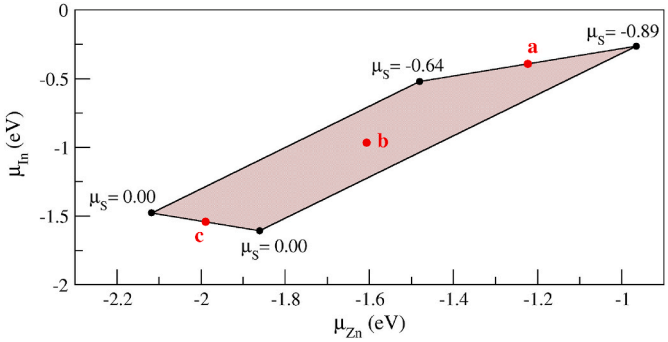

Fig. 2. Two dimensional plot of chemical potentials of Zn and In. The shade area represents all possible values of chemical potentials associated with Eqs. (4) and (5), which are referenced to their natural phases. (For interpretation of the references to colour in this figure legend, the reader is referred to the Web version of this article.)

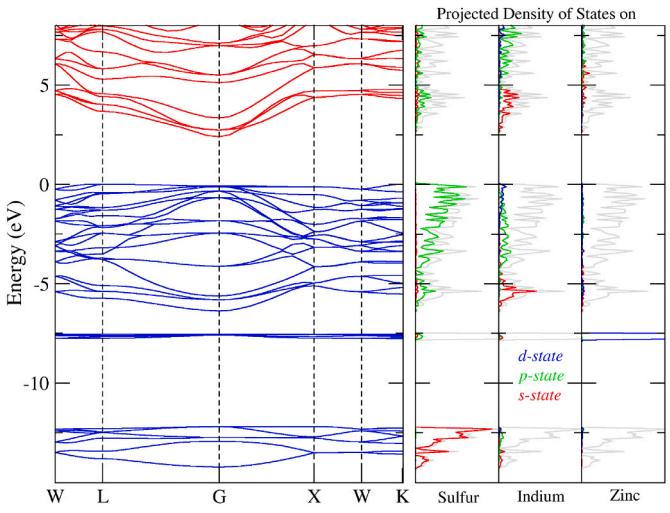

Fig. 3. Band structures of cubic-$ZnIn_2S_4$ (left panel) and the projected density of states on Zn, In, and S atoms (right panel). In the plot, Fermi-level is set to zero. On the right panel, the red, green, and blue lines represent *s*, *p*, and *d* states projected on each atom and the grey line shows the total density of states. (For interpretation of the references to colour in this figure legend, the reader is referred to the Web version of this article.)

does not require any band gap tuning parameter, provides a good agreement with the experimental values; indicating a good accuracy of our calculated approach. Fig. 3 reveals that the hole effective mass of $ZnIn_2S_4$ is significantly large due to a small curvature of the valence band edge. In opposite, the electron effective mass is light due to a high curvature of the conduction band edge. The calculated effective masses for hole and electron are 1.90 and 0.295 m_e, respectively. In the right panel of Fig. 3, the red, green, and blue lines represent *s*, *p*, and *d* density of states projected on each atom, respectively. It is clearly seen that VBM is mainly composed of S-*p* states, while CBM is a hybridization of Zn-*s*, In-*s*, and S-*p* states. Once electrons in valence band are photo-excited, these photo-generated electrons can then easily move to the surface due to this hybridization and the mobility of the photo-generated electrons is significantly high due to its low electron effective mass.

4. Native point defects in cubic-$ZnIn_2S_4$

As illustrated in Eq. (2), the formation energy of defects directly depends on their chemical potentials as described in section 2.2. The illustration of chemical potentials in 2D-plot is depicted in Fig. 2, on which S-poor, S-mid, and S-rich growth conditions are labeled by *a*, *b*, and *c*, respectively. Then, we considered the defect formation energies under three selected conditions to determine the dependence of formation energies under different growth conditions. Fig. 4 illustrates the defect formation energies as a function of Fermi energy under S-poor, S-mid, and S-rich growth conditions. The slope and kink of each line correspond to the charge state and transition level of each defect, respectively. In the plot, the possible range of Fermi energy is equal to the calculated energy gap of cubic-$ZnIn_2S_4$, which is 2.39 eV. Next, all native point defects including vacancies, interstitial defects, and substitution (antisite) defects are discussed.

4.1. Vacancy defects

It is well-known that vacancies are the dominant defects in several photocatalytic materials [45–48] and these defects could significantly affect their electrical properties resulting in enhancing/degrading the photocatalytic performance of materials. We then investigated the likelihood of zinc vacancy (V_{Zn}), indium vacancy (V_{In}) and sulfur vacancy (V_S) formations under different growth conditions by considering their formation energies as illustrated in Fig. 4. It is found that V_{Zn} defect is a deep acceptor with two defect transition levels: $\varepsilon(0/-1) = 0.30$ eV and $\varepsilon(-1/-2) = 0.41$ eV. Under *n*-type condition, (i.e., Fermi level is close to CBM), the existence of V_{Zn} defect is likely due to its low formation energy, whereas the formation of V_{Zn} defect under *p*-type conditions (i.e., Fermi level is close to VBM) is unlikely owning to its high formation energy. Regarding V_S defect, it is a deep donor with one defect transition level at $\varepsilon(+2/0) = 2.03$ eV and it shows a negative-*U* behavior due to a large local lattice relaxation between neutral and 2+ charge state. In addition, the formation energy of V_S defect is quite low under *p*-type condition; indicating that V_S defect is likely to exist only under *p*-type condition. The deep trap states in the band gap associated with V_{Zn} and V_S defects could result in shorten electrons/holes lifetime as well as enhance radiative recombination. Due to various possible oxidation states of indium, we found that V_{In} is an amphoteric defect, *i.*

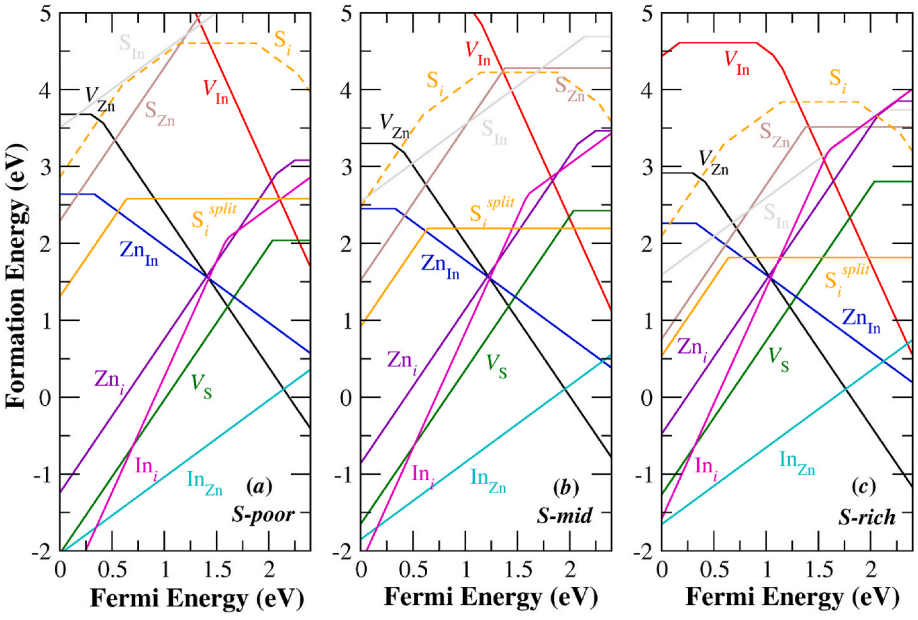

Fig. 4. Illustration of defect formation energy as a function of Fermi energy under (a) S-poor, (b) S-mid, and (c) S-rich growth conditions. The slope of each line indicates the charge state of each defect. The VBM is set to zero and the Fermi energy is extended to the calculated band gap of 2.39 eV.

e., it can be donor or acceptor depending on the Fermi level position as depicted in Fig. 4. The defect transition levels associated with V_{In} are $\varepsilon(+1/0) = 0.17$ eV, $\varepsilon(0/-1) = 0.91$ eV, $\varepsilon(-1/-2) = 1.07$ eV, and $\varepsilon(-2/-3) = 1.16$ eV. It is clearly seen that the formation energy of V_{In} is relatively high throughout Fermi level under all growth conditions considered. This indicates that the existence of V_{In} defects in cubic-$ZnIn_2S_4$ is unlikely.

As mentioned above, under *n*-type condition, the formation energy of V_S defect is very high under all growth conditions; indicating that the existence of V_S defect in cubic-$ZnIn_2S_4$ is unlikely or it would exist in a low concentration. This agrees well with the recent work by J. Wang [28] reported that the electron spin resonance (ESR) signal associated with V_S defect in cubic-$ZnIn_2S_4$ sample could not be detected. In opposite, the formation energy of V_{Zn} defect under all growth conditions turns to be lower when the Fermi level is close to CBM as depicted in Fig. 4. Consequently, the formation of V_{Zn} defect is likely under *n*-type growth condition and it becomes a dominant compensating defect or electron acceptor. Recently, X. Jiao synthesized $ZnIn_2S_4$ samples under two specific growth conditions to create a high and low concentration of V_{Zn} defects in samples [29]. They claimed that the formation of V_{Zn} defects could act as an electron acceptor, and it helped to boost the electron-hole separation efficiency. This agrees well with the low formation energy of V_{Zn} defect under *n*-type condition. However, the enhancement of photocatalytic activity by the formation of compensating defect V_{Zn} is still ambiguous and more discussion will be provided in the last section. Further, we will show later that the pinned Fermi-level of cubic-$ZnIn_2S_4$ under all considered growth conditions is relatively high; indicating that cubic-$ZnIn_2S_4$ is a native *n*-type material.

4.2. Interstitial defects

In this section, we investigated the likelihood of interstitial defects, including Zn_i, In_i and S_i atoms at octahedral site as depicted in the lower part of Fig. 1. Further, we also considered S split-interstitial defect (S_i^{split}), in which two S atoms share the same lattice site as shown in Fig. 1. It is found that Zn_i defect is a shallow donor with two defect transition level at $\varepsilon(+2/+1) = 2.08$ eV and $\varepsilon(+1/0) = 2.25$ eV. In_i defect is also a donor with two defect transition levels at $\varepsilon(+3/+2) = 1.58$ eV and $\varepsilon(+2/+1) = 1.62$ eV. As illustrated in Fig. 4, both Zn_i and In_i defects have significantly high formation energy under *n*-type condition, which is like the case of V_S defect. Therefore, Zn_i and In_i defects cannot be a source of *n*-type conductivity in cubic-$ZnIn_2S_4$. Regarding sulfur interstitial, S_i^{split} defect is a deep donor with defect transition levels at $\varepsilon(+2/+1) = 0.63$ eV and $\varepsilon(+1/0) = 0.65$ eV, while S_i at octahedral site is an amphoteric with defect transition level at $\varepsilon(+2/+1) = 0.60$ eV, $\varepsilon(+1/0) = 1.15$ eV, $\varepsilon(0/-1) = 1.88$ eV and $\varepsilon(-1/-2) = 2.28$ eV. Both S_i and S_i^{split} defects have relatively high formation energy compared to other defects. Due to the high formation energies of interstitial defects, the existence of interstitial defects in cubic-$ZnIn_2S_4$ is unlikely or they would exist in a very low concentration. Therefore, the influence of interstitial defects on the photocatalytic activity of $ZnIn_2S_4$ can be neglected.

4.3. Substitutional defects

We investigated the likelihood of substitutional (antisite) defects, including Zn substitution for In atom (Zn_{In}), In substitution for Zn atom (In_{Zn}), S substitution for Zn atom (S_{Zn}) and S substitution for In atom (S_{In}). The formation energies of substitutional defects are also depicted in Fig. 4. As we expected, the formation energies of both S_{Zn} and S_{In} are relatively high under all considered growth conditions. This is due to the large differences in the ionic radius and electronegativity between the host and substituted atoms. We then concluded that the anion substitution for cation and vice versa is unlikely to exist in cubic-$ZnIn_2S_4$ as well as other materials. Interestingly, this ternary sulfide material has two cation species with difference oxidation states, *i.e.*, Zn^{2+} and In^{3+} and we suspected whether these two cations can swap their positions. We then investigated the likelihood of antisite between Zn and In atoms. It is found that In_{Zn} defect is a shallow donor without creating any defect-level in the bandgap, whereas Zn_{In} defect is a deep acceptor with one defect level at $\varepsilon(0/-1) = 0.33$ eV. Interestingly, the formation energy of In_{Zn} defect is significantly low under all growth conditions, whereas that of Zn_{In} defect is relatively high under *p*-type condition and turns to be lower under *n*-type condition.

As mentioned above, In_{Zn} defect, which is a donor, has the lowest formation energy under all growth conditions compared with other donor defects. This indicates that In_{Zn} defect can be a source of *n*-type conductivity in cubic-$ZnIn_2S_4$. As shown in Fig. 4, In_{Zn} and V_{Zn} defect are the dominant donor and acceptor, respectively, and these two defects determine the efficiency of materials. For example, under some certain growth condition, such as Fig. 4a, In_{Zn} defect has the lowest formation energy until Fermi-level is above 2.15 eV, at which the compensating defect V_{Zn} turns to have the lowest energy. The crossing line between In_{Zn} and V_{Zn} defects is close to CBM resulting in a good *n*-type conductivity of material. Therefore, the synthesis of cubic-$ZnIn_2S_4$ under this condition should provide a good electrical conductivity, and then the photo-generated electrons should easily transfer to the surface and participate in the redox reactions. This provides a good photocatalytic activity of $ZnIn_2S_4$ sample. In next section, the position of Fermi-level will be again discussed by considering charge neutrality condition.

4.4. Charge neutrality condition

As mentioned before, the electrical conductivity of materials can be determined from their pinned Fermi-level, which can be calculated from charge neutrality condition: $p - n + \sum q\,C(D^q) = 0$, where p and n are the concentration of intrinsic hole and electron, respectively, and $C(D^q)$ is the concentration of defect D at charge state q. The calculated pinned Fermi-level of good *p*-type materials should be close to VBM, whereas that of good *n*-type materials should approach CBM. Regarding cubic-$ZnIn_2S_4$, we found that the calculated pinned Fermi-levels are ~2.13, 1.94 eV, and 1.75 eV for S-poor, S-mid, and S-rich growth conditions, respectively. We noted that only the defects with low formation energy were taken into consideration, *i.e.*, In_{Zn} and V_{Zn} defects. The calculated pinned Fermi-levels under all growth conditions seem to be adjacent to CBM; indicating that cubic-$ZnIn_2S_4$ materials is a native *n*-type material and the synthesis of this material under S-poor growth condition should provide the best electrical conductivity compared to other growth conditions.

As mentioned before, X. Jiao reported that V_{Zn} defects act as electron acceptors and it helps to boost the electron-hole separation and photocatalytic efficiencies [29]. However, the increase of V_{Zn} defect, which is electron killer, should instead reduce the number of photo-generated electron and deteriorate the photocatalytic efficiency of $ZnIn_2S_4$ sample. In this case, we suggested that the boost of V_{Zn} defect under some growth conditions could help increasing the formation of In_{Zn} defect, which is a shallow donor. This results in the enhancement of photo-generated carriers as well as the photocatalytic activity of $ZnIn_2S_4$ sample under some growth conditions.

Previously, the native point defects in anatase-TiO_2 and rutile-TiO_2 have been reported, and the main conclusions of the dominant native point defects in both structures are analogous [31,32]. This can be understood by considering the total ground state energy of both structures and their chemical potentials used in defect calculations. The crystal structures of anatase and rutile TiO_2 are hexagonal and cubic, respectively, and the total ground state energies of both structures are close to each other. Therefore, the set of chemical potentials used in defect calculations for both structures is almost similar. In addition, the local environments around Ti and O in both structures, such as bond distance and angle, are not much difference. This is a reason why the calculations of defects in rutile-TiO_2 and anatase-TiO_2 provide analogous results.

Turning to our case, $ZnIn_2S_4$ can crystalize in cubic and hexagonal polymorphs and the total ground state energies of different polymorphs are not much difference. Consequently, the set of chemical potentials used in defect calculations for cubic and hexagonal phases is mostly similar. The local environments of Zn are 4-fold coordinated to S atoms in both structures. However, in hexagonal phase, In are 4-fold and 6-fold coordinated to S atoms, in opposite to cubic phase, which is only 6-fold coordination. This suggested the lower formation energy of V_{In} (4-fold) in hexagonal phase compared to that in cubic phase. In addition, it implies that In prefers to bond with not only six S atoms, but also with four S atoms. This is a reason why the formation of In_{Zn} defect in cubic phase, which is 4-fold coordination, is likely. Consequently, it is reasonable to suggest that the existence of In_{Zn} defect in hexagonal phase is also likely. In addition, there are more inequivalent sites in hexagonal phase needed to be considered, which requires more computational time. However, we believed that the main conclusions obtained from cubic-$ZnIn_2S_4$ could be applied for the case of hexagonal phase. We then conclude that the photocatalytic activity of undoped $ZnIn_2S_4$ sample is determined by the dominant donor In_{Zn} and compensating V_{Zn} defects. Further, owning to the high pinned Fermi-level of $ZnIn_2S_4$ under all growth conditions, other *n*-type doping elements in $ZnIn_2S_4$ are suggested to enhance its photocatalytic performance.

5. Conclusion

First-principles calculations with accurate HSE06 functional were used to investigate the crystal and electronic structures of bulk and defective cubic-$ZnIn_2S_4$. We found that cubic-$ZnIn_2S_4$ is an indirect bandgap with the calculated energy gap of 2.39 eV. The VBM and CBM are located at K and Γ points, respectively. The effect of growth conditions on photocatalytic performance was examined by calculating the defect formation energy under different growth conditions varying from S-rich to S-poor. Our results revealed that the In_{Zn} antisite defect is a dominant donor defect, which is a main source of photo-induced carriers in undoped $ZnIn_2S_4$. However, the photocatalytic activity of $ZnIn_2S_4$ is deteriorated by the formation of compensating defect V_{Zn}, which could trap the photo-induced carriers. The calculated pinned Fermi-level of $ZnIn_2S_4$ is relatively high under all growth conditions considered; indicating that $ZnIn_2S_4$ is a native *n*-type material. We further proposed that the In_{Zn} antisite and V_{Zn} defects would be the dominant donor and compensating defects in hexagonal-$ZnIn_2S_4$. In addition, *n*-type doping elements are also suggested to improve its photocatalytic performance.

Credit Author Statement

Siwakorn Sukharom: Data curation, Investigation, Visualization Adisak Boonchun: Resources Pakpoom Reunchan: Resources Sirichok Jungthawan: Resources Sukit Limpijumnong: Resources. Jiraroj T-Thienprasert: Conceptualization, Writing – review & editing, Supervision

Data availability

Datasets related to this article can be found at https://doi.org/10.17632/55sf4ykttj.1, an open-source online data repository hosted at Mendeley Data (T-Thienprasert, 2021).

Declaration of competing interest

The authors declare that they have no known competing financial interests or personal relationships that could have appeared to influence the work reported in this paper.

Acknowledgement

This work was supported by (i) Suranaree Univerisity of Technology (SUT), (ii) Thailand Science Research and Innovation (TSRI), and (iii) National Science, Research and Innovation Fund (NSRF). S. S. acknowledges financial support from the Development and Promotion of Science and Technology Talents Project (DPST). J. T. is supported by Kasetsart University Research and Development Institute (KURDI), Bangkok, Thailand.

References

[1] T.A. Gad-Allah, K. Fujimura, S. Kato, S. Satokawa, T. Kojima, J. Hazard Mater. 154 (2008) 572–577.
[2] M. Gondal, X. Chang, Z. Yamani, Chem. Eng. J. 165 (2010) 250–257.
[3] M. Sun, D. Li, W. Zhang, Z. Chen, H. Huang, W. Li, Y. He, X. Fu, J. Solid State Chem. 190 (2012) 135–142.
[4] T. Peng, D. Ke, J. Xiao, L. Wang, J. Hu, L. Zan, J. Solid State Chem. 194 (2012) 250–256.
[5] G. Patrinoiu, M. Tudose, J.M. Calderón-Moreno, R. Birjega, P. Budrugeac, R. Ene, O. Carp, J. Solid State Chem. 186 (2012) 17–22.
[6] M.R. Hoffmann, S.T. Martin, W. Choi, D.W. Bahnemann, Chem. Rev. 95 (1995) 69–96.
[7] A. Fujishima, T.N. Rao, D.A. Tryk, J. Photochem. Photobiol., A C 1 (2000) 1–21.
[8] C. Chen, W. Ma, J. Zhao, Chem. Soc. Rev. 39 (2010) 4206–4219.
[9] D. Chen, D. Yang, Q. Wang, Z. Jiang, Ind. Eng. Chem. Res. 45 (2006) 4110–4116.
[10] S. Ouyang, J. Ye, J. Am. Chem. Soc. 133 (2011) 7757–7763.
[11] D. He, L. Wang, D. Xu, J. Zhai, D. Wang, T. Xie, ACS Appl. Mater. Interfaces 3 (2011) 3167–3171.
[12] W. Zhou, H. Liu, J. Wang, D. Liu, G. Du, J. Cui, ACS Appl. Mater. Interfaces 2 (2010) 2385–2392.
[13] L. Zhang, L. Yin, C. Wang, N. Lun, Y. Qi, ACS Appl. Mater. Interfaces 2 (2010) 1769–1773.
[14] J. Song, T. Jiang, G. Ji, W. Zhang, X. Cheng, W. Weng, L. Zhu, X. Xu, RSC Adv. 5 (2015) 95943–95952.
[15] T. Liu, L. Wang, X. Lu, J. Fan, X. Cai, B. Gao, R. Miao, J. Wang, Y. Lv, RSC Adv. 7 (2017) 12292–12300.
[16] T.D. Savić, M.V. Carević, M.N. Mitrić, J.Ž. Kuljanin-Jakovljević, N.D. Abazović, M. I. Čomor, J. Photochem. Photobiol. Chem. 388 (2020) 112154.
[17] Y. Chen, R. Huang, D. Chen, Y. Wang, W. Liu, X. Li, Z. Li, ACS Appl. Mater. Interfaces 4 (2012) 2273–2279.
[18] M. Sriram, P. McMichael, A. Waghray, P. Kumta, S. Misture, X.-L. Wang, J. Mater. Sci. 33 (1998) 4333–4339.
[19] S. Yang, L. Li, W. Yuan, Z. Xia, Dalton Trans. 44 (2015) 6374–6383.
[20] Y. Chen, S. Hu, W. Liu, X. Chen, L. Wu, X. Wang, P. Liu, Z. Li, Dalton Trans. 40 (2011) 2607–2613.
[21] J. Chen, F. Xin, X. Yin, T. Xiang, Y. Wang, RSC Adv. 5 (2015) 3833–3839.
[22] S. Shen, L. Zhao, X. Guan, L. Guo, J. Phys. Chem. Solid. 73 (2012) 79–83.
[23] S. Shen, X. Chen, F. Ren, C.X. Kronawitter, S.S. Mao, L. Guo, Nanoscale Res. Lett. 6 (2011) 1–6.
[24] S. Shen, L. Zhao, Z. Zhou, L. Guo, J. Phys. Chem. C 112 (2008) 16148–16155.
[25] D. Jing, M. Liu, L. Guo, Catal. Lett. 140 (2010) 167–171.
[26] Y. Yu, G. Chen, G. Wang, Z. Lv, Int. J. Hydrogen Energy 38 (2013) 1278–1285.
[27] Z. Mei, S. Ouyang, D.-M. Tang, T. Kako, D. Golberg, J. Ye, Dalton Trans. 42 (2013) 2687–2690.
[28] J. Wang, Y. Chen, W. Zhou, G. Tian, Y. Xiao, H. Fu, H. Fu, J. Mater. Chem. 5 (2017) 8451–8460.
[29] X. Jiao, Z. Chen, X. Li, Y. Sun, S. Gao, W. Yan, C. Wang, Q. Zhang, Y. Lin, Y. Luo, J. Am. Chem. Soc. 139 (2017) 7586–7594.
[30] S. Zhang, X. Liu, C. Liu, S. Luo, L. Wang, T. Cai, Y. Zeng, J. Yuan, W. Dong, Y. Pei, ACS Nano 12 (2018) 751–758.
[31] H. Peng, Phys. Lett. 372 (2008) 1527–1530.
[32] S. Na-Phattalung, M.F. Smith, K. Kim, M.-H. Du, S.-H. Wei, S.B. Zhang, S. Limpijumnong, Phys. Rev. B 73 (2006) 125205.
[33] G. Kresse, D. Joubert, Phys. Rev. B 59 (1999) 1758.
[34] G. Kresse, J. Furthmüller, Comput. Mater. Sci. 6 (1996) 15–50.
[35] G. Kresse, J. Hafner, J. Phys. Condens. Matter 6 (1994) 8245.
[36] P.E. Blöchl, Phys. Rev. B 50 (1994) 17953.
[37] C. Freysoldt, J. Neugebauer, C.G. Van de Walle, Phys. Status Solidi B 248 (2011) 1067–1076.
[38] C. Freysoldt, J. Neugebauer, C.G. Van de Walle, Phys. Rev. Lett. 102 (2009), 016402.
[39] H.J. Monkhorst, J.D. Pack, Phys. Rev. B 13 (1976) 5188.
[40] R.P. Feynman, Phys. Rev. 56 (1939) 340–343.
[41] K.-J. Range, W. Becker, A. Weiss, Z. Naturforsch. B Chem. Sci. 24 (1969) 811–812.
[42] S. Zhang, J.E. Northrup, Phys. Rev. Lett. 67 (1991) 2339.
[43] J.E. Northrup, S. Zhang, Phys. Rev. B 50 (1994) 4962.
[44] Y.J. Zhang, H.M. Tang, S.-P. Gao, Phys. Status Solidi B 257 (2020) 1900485.
[45] P. Pakeetood, P. Reunchan, A. Boonchun, S. Limpijumnong, R. Munprom, R. Ahuja, J. T-Thienprasert, J. Phys. Chem. C 123 (2019) 14508–14516.

[46] J. T-Thienprasert, S. Limpijumnong, Appl. Phys. Lett. 107 (2015) 221905.
[47] A. Janotti, J. Varley, P. Rinke, N. Umezawa, G. Kresse, C.G. Van de Walle, Phys. Rev. B 81 (2010), 085212.
[48] A. Janotti, C.G. Van de Walle, Phys. Rev. B 76 (2007) 165202.

Further reading

[49] J. T-Thienprasert, Optimized POSCAR files for a paper entitled "Effect of native point defects on the photocatalytic performance of ZIS", Mendeley Data V1 (2021), 10.17632/55sf4ykttj.1.